Journal of the Ceramic Society of Japan 123 [9] 845-852 2015 Special Article
The 69th CerSJ Awards for Academic Achievements in Ceramic Science and Technology: Review

Diverse structures of mixed-metal oxides containing rare earths and their magnetic properties

Yukio HINATSU†

Division of Chemistry, Hokkaido University, Sapporo 060–0810, Japan

The solid state chemistry of mixed-metal oxides containing rare earths (4*f* elements) and 4*d* or 5*d* transition elements has attracted a great deal of interest, because these materials adopt a diverse range of structures and show a wide range of electronic properties due to 4*f* and 4*d* (or 5*d*) electrons. We have focused our attention on the structural chemistry and magnetic properties of perovskite-type oxides with the general formula $A_nLnM_{n-1}O_{3n}$ (A = Ca, Sr, Ba; Ln = rare earths; M = Ru, Ir; n = 1–4). Their structures are controlled by changing the ratio of the Ln and M ions, and peculiar magnetic properties and magnetic structures have been investigated by magnetic susceptibility, specific heat and neutron diffraction measurements.

©2015 The Ceramic Society of Japan. All rights reserved.

Key-words : Magnetic properties, Perovskite, Rare earth, Magnetic structure, Ruthenium, Iridium

[Received April 6, 2015; Accepted July 7, 2015]

1. Introduction

It is well known that the most stable oxidation state of rare earth ions is trivalent, and the electron configuration of Ln^{3+} ions is $[Xe]4f^n$ ([Xe]: xenon electronic core). The magnetic properties of the rare earth ions are fascinating for the reason of their systematic variety and intelligible complexity. They are highly localized electrons, and the shielding by the surrounding 5s and 5p electrons in the outer shell makes the magnetic interactions between 4f electrons in the condensed matter very weak, compared with those between d electrons. In fact, many of the rare earth oxides order magnetically when the temperature is decreased down to below 4 K.

One of the most challenging problems in the modern chemistry of rare earth compounds is to find a compound in which strong magnetic super-exchange interactions between 4f electrons exist, which give rise to a long-range magnetic ordering at relatively high temperatures, and to elucidate their mechanism.

We have been focusing our attention on the crystal structures of the perovskite-type compounds containing rare earth ions. The rare earth ion is relatively large and tends to adopt a high coordination number. Therefore, the rare earth ion usually sits at the A site of the perovskite-type oxides ABO_3. Not the A site ions but the B site ions normally determine the physical properties of the perovskites.[1)]

In this review article, we describe the preparation and structures of $ALnO_3$ (A = alkaline earth elements; Ln = rare earths) and $A_nLnM_{n-1}O_{3n}$ (n = 2–4) in which the rare earth elements are situated at the B-site of the perovskite-type oxides. Through magnetic susceptibility, specific heat, and neutron diffraction measurements, their magnetic properties have been studied.

2. $ALnO_3$ (A = Ba, Sr; Ln = Pr, Tb)

Among seventeen rare earth elements, cerium, praseodymium and terbium have the tetravalent state in addition to the trivalent state. The electron configuration of Pr^{4+} and Tb^{4+} ions are $[Xe]4f^1$ and $[Xe]4f^7$ (half-filled 4f shell), respectively. These electronic configurations simplify the analysis of the electronic properties of 4f electrons in solids, and it is easy to compare the experimental results with theoretical calculations.

Since the ionic radius of tetravalent rare earths is considerably smaller than that of the corresponding trivalent rare earths, Pr^{4+} and Tb^{4+} ions should be situated at the B-site of the perovskite. Under flowing oxygen atmosphere, $BaPrO_3$, $BaTbO_3$, $SrPrO_3$ and $SrTbO_3$ could be prepared. They are crystallized orthorhombically (space group: Pnma).[2)–5)] Electron paramagnetic resonance measurements clearly showed that the oxidation state of Pr and Tb is in the tetravalent state.[6),7)] Magnetic susceptibility, specific heat and neutron diffraction measurements show that $BaPrO_3$, $SrTbO_3$ and $BaTbO_3$ order magnetically at relatively high temperatures, i.e., 11.7, 32.0, and 33.4 K, respectively.[5),7),8)] **Figure 1** shows the temperature dependence of the magnetic susceptibility for $SrTbO_3$ and $BaTbO_3$. X-ray diffraction measurements show that Pr–O–Pr (Tb–O–Tb) is almost linearly aligned in their structures, which results in the strong magnetic super-exchange interaction via oxygen atoms. For the case of $SrPrO_3$, the bond angle of Pr–O–Pr is 140° and no magnetic ordering has been observed down to 1.8 K.[4)]

Magnetic structures for any of these compounds is the G-type one from their neutron diffraction measurements. **Figure 2** shows the magnetic structure of $SrTbO_3$ measured at 2.0 K.[5)]

3. Double perovskites A_2LnMO_6 (A = Ba, Sr, Ca; M = Ru)

The perovskites have the flexibility of chemical composition and the possibility of combination of many kinds of ions. By selecting large alkaline earth elements such as Sr and Ba at the A site atoms in the ABO_3, one can accommodate the rare earth (Ln) with smaller transition elements (M) at the 6-coordinate B sites. Since the size of the *Ln* and *M* cations are sufficiently different, they are regularly ordered over the six-coordinate *B* sites.

Since highly oxidized cations from the second or third transition series sometimes show quite unusual magnetic behavior, many studies have been performed on the preparation and magnetic properties of double perovskite oxides containing both rare

† Corresponding author: Y. Hinatsu; E-mail: hinatsu@sci.hokudai.ac.jp

©2015 The Ceramic Society of Japan
DOI http://dx.doi.org/10.2109/jcersj2.123.845

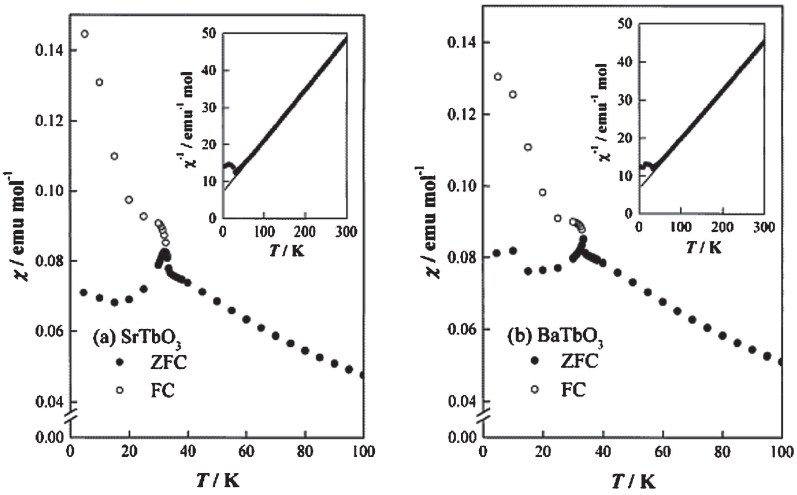

Fig. 1. Temperature dependence of the magnetic susceptibility for (a) $SrTbO_3$ and (b) $BaTbO_3$. The inset shows the temperature dependence of the reciprocal ZFC susceptibility and the Curie–Weiss fitting.

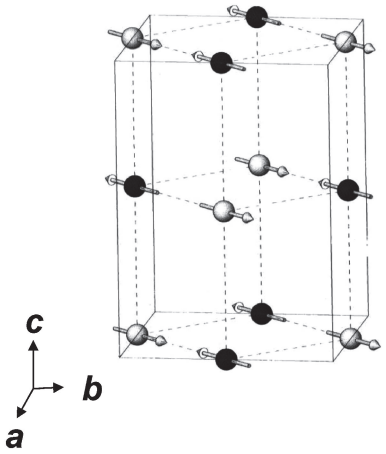

Fig. 2. Magnetic structure of $SrTbO_3$ measured at 2.0 K.

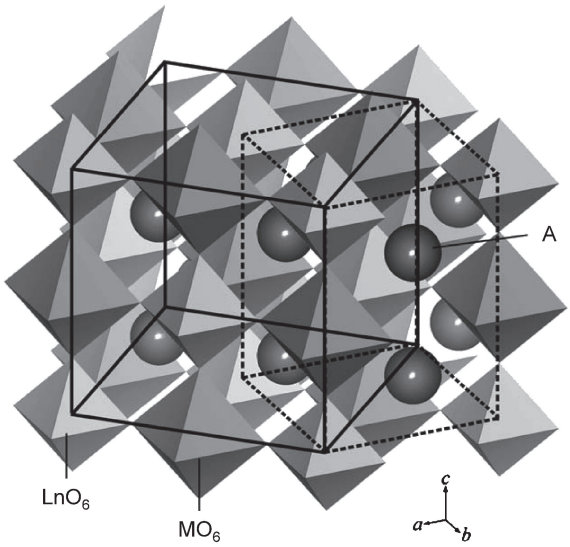

Fig. 3. The relationship between monoclinic and cubic double perovskites A_2LnMO_6. Solid and dotted lines show the cubic cell and the monoclinic cell, respectively.

earth and such transition metals, A_2LnMO_6 (A = Sr, Ba; Ln = rare earths; M = Ru, Os, Ir, Re).[9)–26)] Among them, magnetic properties of pentavalent ruthenium-containing oxides have aroused a great deal of interest, because the Ru^{5+} ion has the largest possible spin (S = 3/2).

The Rietveld analyses of their X-ray diffraction patterns for A_2LnRuO_6 compounds show that for A = Ba, the compounds with large rare earths (Ln = Pr, Nd) adopt a monoclinic unit cell (space group $P2_1/n$) and those with small rare earths (Ln = Sm–Lu) adopt a cubic unit cell (space group Fm-3m). **Figure 3** shows their schematic structures. For A = Sr, any of these compounds adopt the monoclinic unit cell (space group $P2_1/n$). The structural analysis show that the Ln and Ru ions are arranged in an alternating manner (NaCl-type). For Ca_2LnRuO_6, X-ray diffraction measurements show that Ca^{2+} ions partially occupy the B-site, i.e., Ca^{2+} and Ln^{3+} ions are partially disordered at the A-site and half of the B-site of the perovskite ABO_3, and that Ca^{2+}/Ln^{3+} and Ru^{5+} ions located at the B site are regularly ordered.[27)] Therefore, these compounds should be represented by $Ca_{2-x}Ln_x$-$[Ln_{1-x}Ca_x]RuO_6$. The ratio of the Ln^{3+} ion located at the A-site varies with its ionic radius, as shown in **Fig. 4**.

All the A_2LnRuO_6 compounds prepared in this study show an antiferromagnetic transitions at low temperatures. **Figure 5** shows the antiferromagnetic transition temperature for A_2LnRuO_6

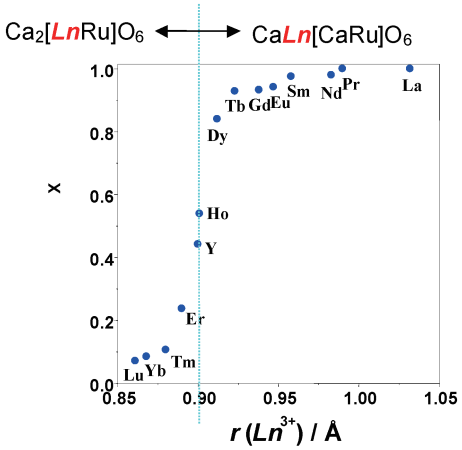

Fig. 4. The ratio of the Ln^{3+} ions at the A-site in the double perovskite A_2LnRuO_6 (x) against the Ln^{3+} radius.

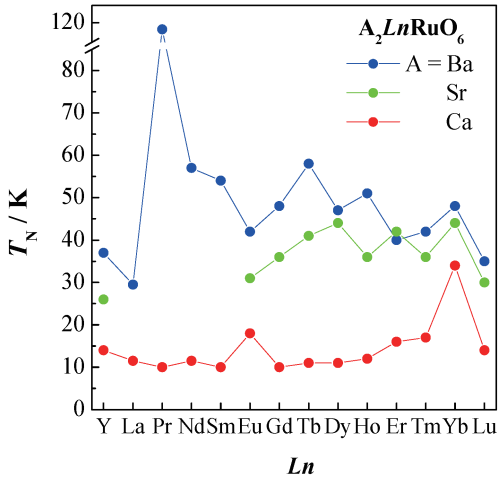

Fig. 5. The Néel temperatures (T_N) of A_2LnRuO_6.

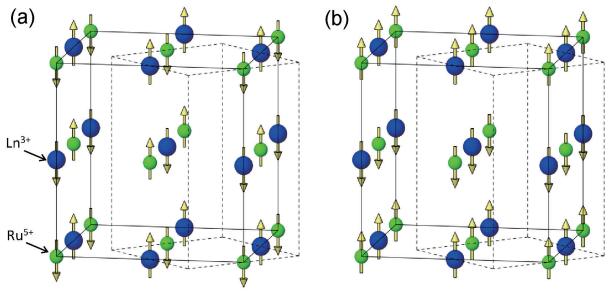

Fig. 6. Schematic magnetic structures of (a) A_2LnRuO_6 (Ln = Tb, Ho, Er, Tm) and (b) A_2LnRuO_6 (Ln = Pr, Nd, Yb).

against the Ln (atomic number). For A = Ba and Sr compounds, the Néel temperatures of the A_2LnRuO_6 (Ln ≠ Y, La, Eu) compounds are higher than those for Ln = Y, La, Eu compounds. This fact indicates that the magnetic transition is mainly due to the magnetic cooperative phenomena between Ru^{5+} ($4d^3$) and Ln^{3+} ($4f^n$) ions. When the A-site cation is changed from Ba to Sr to Ca, the Néel temperature for A_2LnRuO_6 compounds decreases considerably. With decreasing the size of A-site cation, the alignment of Ln–O–Ru deviates from 180°, which results in weakening the magnetic super-exchange interaction between f and d electrons via oxygen atoms. In the case of A =Ca, the Néel temperatures for Ln = La–Ho compounds are nearly constant, which reflects the fact that the B-site cations are Ru and Ca.

Neutron diffraction measurements show that the magnetic structures of these compounds are based on the type I ordering of Ru^{5+} and Ln^{3+} ions and schematic magnetic structures of A_2LnRuO_6 are shown in **Fig. 6**. The A_2LnRuO_6 (Ln = Tb, Ho, Er, Tm) compounds adopt the magnetic structure (a), while the A_2LnRuO_6 compounds with Pr, Nd, Yb adopt the structure (b).[23] The difference between these magnetic structures is in the arrangement of the magnetic moments of Ln^{3+} and Ru^{5+} ions in the *ab* plane. For example, in the case of Sr_2TbRuO_6, the moments of Ln^{3+} and Ru^{5+} are antiparallel with each other, while they are parallel for Ba_2PrRuO_6. The magnetic structure data are summarized in **Table 1**.

4. Triple perovskites $Ba_3LnM_2O_9$ (M = Ru)

Next, we paid our attention to the structure and magnetic properties of triple perovskite oxides containing rare earth and ruthenium, $Ba_3LnRu_2O_9$.

Table 1. Summary of magnetic properties of A_2LnRuO_6

Ln	A	Type*1	Direction of magnetic moments	μ(Ru)/μ_B	μ(Ln)/μ_B	T_N (K)
La	Ba	III_a	*c*-axis	1.95	—	29.5
Pr	Ba	I_p	*c*-axis	2.0	2.2	117
Nd	Ba	I_p	*ab*-plane	2.2	2.3	57
Tb	Sr	I_a	*c*-axis 20°	2.99	4.98	41
Ho	Sr	I_a	*c*-axis	2.71	6.68	36
	Ba	I_a	*c*-axis	2.9	9.7	51
Er	Sr	I_a	*ab*-plane	2.74	4.59	42
	Ba	I_a	*ab*-plane	2.9	4.3	40
Tm	Sr	I_a	*c*-axis	1.5	1.4	36
	Ba	I_a	*c*-axis	2.13	1.91	42
Yb	Sr	I_p	*c*-axis 20°	3.0	0.92	44
	Ba	I_p	*c*-axis 20°	2.57	1.00	48
Lu	Sr	I	*ab*-plane	2.10	—	30
	Ba	I	*ab*-plane	2.06	—	35
Y	Sr	I	*ab*-plane	1.85	—	26
	Ba	I	*ab*-plane	2.11	—	37

Note: *1 I_p; parallel arrangement of magnetic moments between Ln and Ru ions in the *ab* plane, I_a; antiferromagnetic arrangement.

Structures of perovskite oxides (ABO_3) can be regarded as the stacking of close-packed AO_3 layers and the filling of subsequent octahedral sites by *B*-site ions. The difference in the stacking sequence changes the way of linkage of BO_6 octahedra: the corner-sharing BO_6 in the cubic perovskite (3L: three-layer) with *abc*... sequence, the face-sharing BO_6 in 2L-perovskite (2L: two-layer) with *ab*... sequence, and mixed linkages between the corner- and face-sharing in various intergrowth structures.[28] The stacking sequence is controlled by changing the ratio of the *Ln* and *M* ions. Double perovskites Ba_2LnMO_6 (doubling the formula unit, **Fig. 7**, left) are formed, when the size and/or charge of the *Ln* and *M* cations are sufficiently different and the ratio of Ln:M = 1:1.

When the ratio of *Ln*:*M* is 1:2, triple perovskites $Ba_3LnM_2O_9$ are formed. Ln and Ru ions occupy the corner-sharing and face-sharing sites, respectively, and form the LnO_6 octahedron and the Ru_2O_9 polyhedron. This Ru_2O_9 polyhedron consists of two face-sharing RuO_6 octahedra (Ru_2O_9 dimer)[29] (Fig. 7, middle). The magnetic behavior of this Ru_2O_9 dimer is attractive because of a very short Ru–Ru distance (2.5–2.7 A) in the dimer. Therefore, one expects to find a strong magnetic interaction between Ru ions in the dimer.

From the analysis of the lattice parameters and bond lengths for $Ba_3LnRu_2O_9$, the oxidation state of both Ru and Ln ions is tetravalent for the Ce, Pr, and Tb compounds, i.e., Ba_3Ln^{4+}-$Ru^{4+}{}_2O_9$.[30] On the other hand, the other compounds adopt a valence configuration of $Ba_3Ln^{3+}Ru^{4.5+}{}_2O_9$. Their magnetic properties change widely with Ln ion, and are summarized in **Table 2**. Two kinds of magnetic interactions are important in determining their magnetic properties. One is the magnetic interaction between two Ru ions in the Ru_2O_9 dimer; this brings about a strong antiferromagnetic coupling between the Ru ions, and the characteristic temperature-dependence of the magnetic susceptibilities (a broad maximum above 100 K) is observed for $Ba_3LnRu_2O_9$. **Figures 8**(a) and 8(b) show the magnetic susceptibility vs. temperature curves for $Ba_3LnRu_2O_9$ (Ln = Y, Lu, Pr). Another important interaction is the one between the Ru and Ln ions via the linear Ru–O–Ln pathway, which is in common with the case of double perovskites A_2LnRuO_6. The magnetic transition due to the magnetic ordering of Ln ions has been found

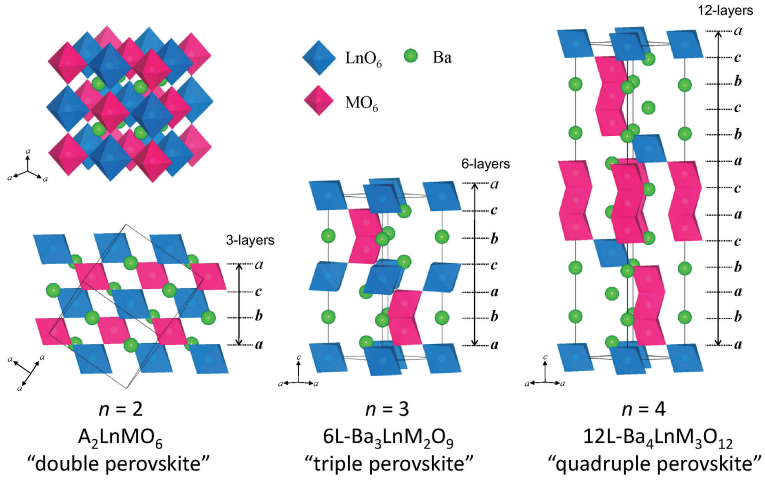

Fig. 7. Crystal structures of $A_nLnM_{n-1}O_{3n}$ (A = Ca, Sr, Ba; M = Ru, Ir; n = 2–4).

Table 2. Summary of magnetic properties of 6L-$Ba_3LnRu_2O_9$

Ln	Oxidation state of Ln	T_a (K)[*1]	T_b (K)[*2]	Neutron diffraction measurements
Y	+3	290	4.5 (AF)	—
La	+3	22	6.0 (AF)	—
Ce	+4	>400	—	—
Pr	+4	380	10.5 (AF)	—
Nd	+3	—	24.0 (F)	Ferromagnetic ordering of Nd^{3+}, 1.65 μ_B/Nd (at 10 K)
Sm	+3	180	12.5 (AF)	—
Eu	+3	135	9.5 (AF)	—
Gd	+3	—	14.8 (AF)	—
Tb	+4	—	9.5 (AF)	Antiferromagnetic ordering of Tb^{4+}, 6.84 μ_B/Tb (at 2.0 K)
Dy	+3	—	27.8 (AF)	—
Ho	+3	—	10.2 (AF)	—
Er	+3	—	6.0 (AF)	—
Tm	+3	—	8.3 (AF)	—
Yb	+3		4.5 (AF)	—
Lu	+3	345	9.5 (AF)	—

Note: [*1]; Temperatures at which a broad maximum was observed in the χ vs T curves due to the magnetic ordering of Ru_2O_9 dimer, [*2]; magnetic ordering of Ln ions.

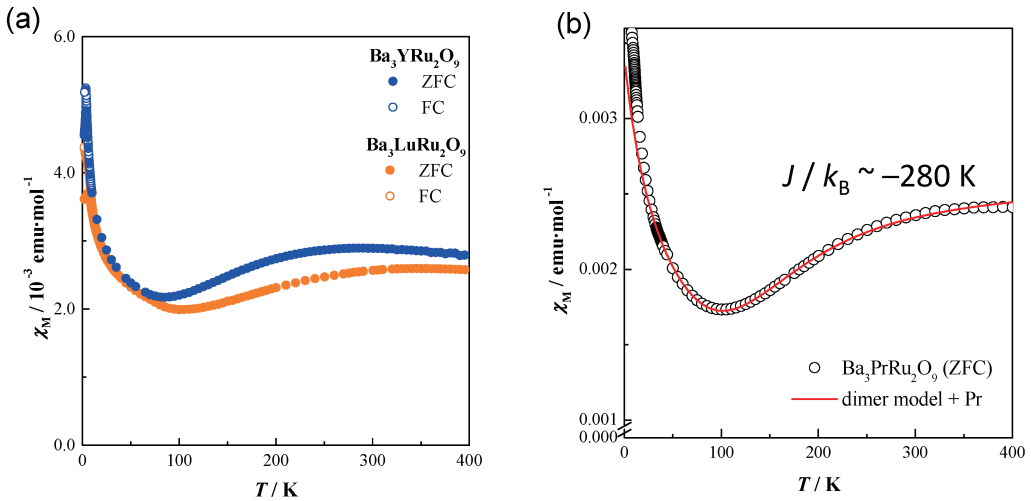

Fig. 8. Temperature dependence of the magnetic susceptibility for (a) $Ba_3LnRu_2O_9$ (Ln = Y, Lu) and (b) $Ba_3PrRu_2O_9$.

in the $Ba_3LnRu_2O_9$ compounds (Ln = magnetic ions) below 10 K.[31] **Figure 9** shows the temperature dependence of the magnetic susceptibility and specific heat for $Ba_3TbRu_2O_9$, and **Fig. 10** depicts its magnetic structure determined at 2.0 K.

5. Quadruple perovskites $Ba_4LnM_3O_{12}$ (M = Ru, Ir)

In the $Ba_3LnM_2O_9$, the ground state of the total spin of the isolated M_2O_9 dimer may be zero, i.e., $S_{dimer} = S_1 + S_2 = 0$, for

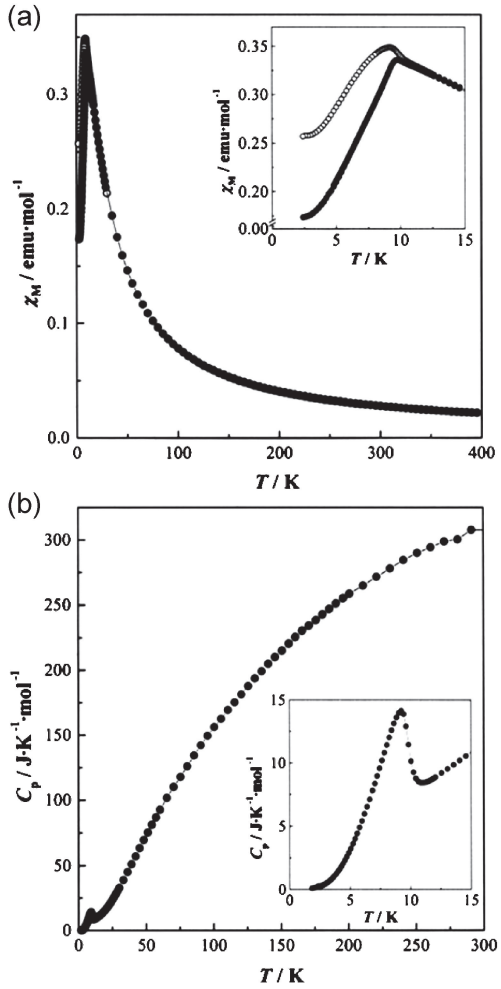

Fig. 9. Temperature dependence of (a) magnetic susceptibility and (b) specific heat for $Ba_3TbRu_2O_9$.

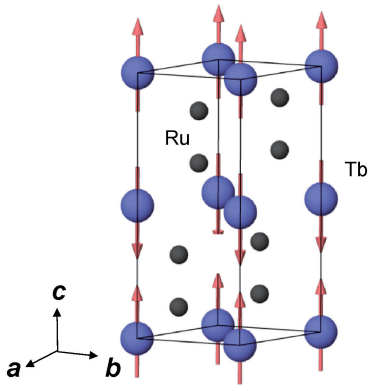

Fig. 10. Magnetic structure of $Ba_3TbRu_2O_9$ at 2.0 K.

the case that the antiferromagnetic coupling exists between the M ions.

Then, we started studies on quadruple perovskites $Ba_4LnM_3O_{12}$ in which the ratio of *Ln*:*M* is 1:3. Three MO_6 octahedra are connected to each other by face-sharing and form a M_3O_{12} trimer. The M_3O_{12} trimers and LnO_6 octahedra are alternately linked by corner-sharing (Fig. 7, right). As shown in this figure, the perovskite-type structure with 12 layers is formed (the stacking sequence: *ababcacabcbc*...).[32)–36)] In this case, the total magnetic

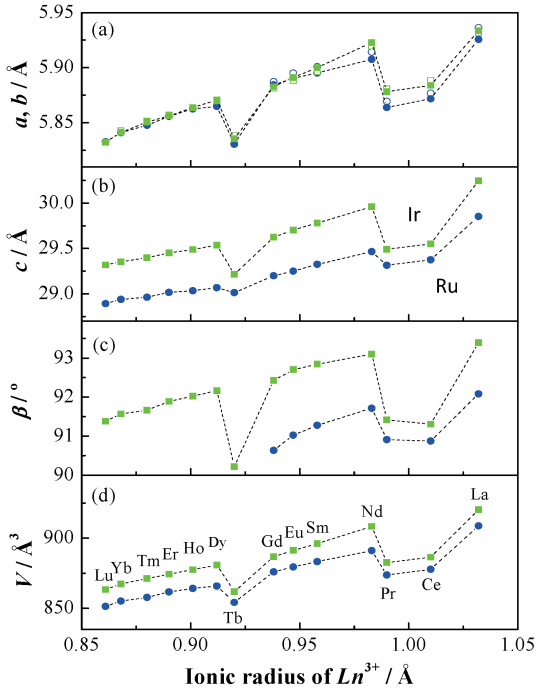

Fig. 11. Variation of lattice parameters and volumes for $Ba_4LnM_3O_{12}$ (M = Ru, Ir) with Ln^{3+} radius.

moment of the M_3O_{12} trimer does not disappear as far as three *M* ions are equivalent in the trimer (i.e., $S_{trimer} = S_1 + S_2 + S_3 \neq 0$), and the ground state of the total spin of the M_3O_{12} trimer should strongly contribute to the magnetic properties of $Ba_4LnM_3O_{12}$.

Quadruple perovskites $Ba_4LnM_3O_{12}$ (*Ln* = La–Nd, Sm–Lu; *M* = Ru, Ir) were prepared as a single phase. The powder X-ray diffraction measurements and their Rietveld analysis show that the $Ba_4LnRu_3O_{12}$ compounds for *Ln* = Tb–Lu have a hexagonal unit cell with space group *R*-3*m* (No.166), while those for Ln = La–Nd, Sm–Gd have a monoclinic unit cell with space group *C*2/*m* (No.12) due to the larger difference in the ionic radius between *Ln* and Ru.[35)] On the other hand, all the iridium compounds $Ba_4LnIr_3O_{12}$ were indexed with the monoclinic unit cell. The *M*–*M* interatomic distances in the M_3O_{12} trimer are 2.4–2.6 Å for both $Ba_4LnRu_3O_{12}$ and $Ba_4LnIr_3O_{12}$ compounds. These distances are much shorter than double the metallic radius of Ru and Ir (2.72 Å),[37)] indicating that strong interactions between *M* ions should exist in the M_3O_{12} trimer.

The lattice parameters and volumes of $Ba_4LnM_3O_{12}$ were plotted against the ionic radius of Ln^{3+} in **Fig. 11**. Except for the compounds having *Ln* = Ce, Pr, and Tb, the lattice parameters *a*, *b*, *c*, and β monotonously increase with the Ln^{3+} ionic radius. However, the values for *Ln* = Ce, Pr, and Tb compounds are considerably smaller than this trend. The Ln–O bond lengths are close to the Ln^{4+}–O^{2-} lengths calculated from Shannon's ionic radii.[38)] These results show that the Ce, Pr, and Tb ions are in the tetravalent state. Therefore, the oxidation states of Ru and Ir are also tetravalent ($Ba_4Ln^{4+}Ru^{4+}{}_3O_{12}$, $Ba_4Ln^{4+}Ir^{4+}{}_3O_{12}$). For other *Ln* ions, the mean oxidation state of Ru and Ir ions is +4.33 ($Ba_4Ln^{3+}Ru^{4.33+}{}_3O_{12}$, $Ba_4Ln^{3+}Ir^{4.33+}{}_3O_{12}$).[39),40)]

5.1 Magnetic properties of $Ba_4Ln^{3+}M^{4.33+}{}_3O_{12}$

Measurements of the magnetic susceptibility for $Ba_4LnM_3O_{12}$ give the contrastive results between the ruthenium-containing compounds $Ba_4LnRu_3O_{12}$ and the iridium-containing compounds $Ba_4LnIr_3O_{12}$, and the results are summarized in **Table 3**. Any of

the $Ba_4Ln^{3+}Ru^{4.33+}{}_3O_{12}$ compounds shows similar magnetic transitions at very low temperatures, whereas $Ba_4Ln^{3+}Ir^{4.33+}{}_3O_{12}$ ($Ln \neq$ La, Lu) compounds are paramagnetic down to 1.8 K.

Magnetic properties of $Ba_4Ln^{3+}Ir^{4.33+}{}_3O_{12}$ clearly show that we have to treat the M ions as the M_3O_{12} trimer to understand their magnetic behavior. Both compounds $Ba_4Ln^{3+}Ir^{4.33+}{}_3O_{12}$ ($Ln =$ La, Lu) are diamagnetic, indicating that the $Ir^{4.33+}{}_3O_{12}$ trimers are diamagnetic. Other compounds $Ba_4Ln^{3+}Ir^{4.33+}{}_3O_{12}$ (i.e., $Ln \neq$ La, Lu) are paramagnetic, and their effective magnetic moments (μ_{eff}) are close to the magnetic moments of Ln^{3+} ions (μ_{Ln}) (see **Table 4**). That is, the contribution of the $Ir^{4.33+}{}_3O_{12}$ trimer to the magnetic properties of $Ba_4LnIr_3O_{12}$ is negligible.

As described above section, the distances between Ir atoms in the Ir_3O_{12} trimer are 2.48–2.60 Å. The short Ir–Ir interatomic distances in the Ir_3O_{12} trimer suggest the overlap of metal d orbitals having lobes along the threefold symmetry axis, which means the formation of molecular orbitals in the Ir_3O_{12} trimer. The electronic structure of Ru_3Cl_{12} with D_{3h} point symmetry has been described.[41] The energy level scheme of Ir_3O_{12} in the $Ba_4LnIr_3O_{12}$ should be similar to the case of Ru_3Cl_{12}, but the degenerated energy levels are expected to be split into more levels due to the monoclinic distortion of the Ir_3O_{12} trimer and to the spin–orbit coupling of the 5d electrons (Ir ions). The electron configuration of the $Ir^{4.33+}{}_3O_{12}$ trimer (the number of 5d electrons is 14) with D_{3h} point symmetry is $(a_{1g})^2(e_g)^4(a_{2u})^2(e_u)^4(e_g)^2$, and the schematic energy level diagrams for the Ir–Ir interactions in the $Ir^{4.33+}{}_3O_{12}$ trimer are illustrated in **Fig. 12**(c). The highest occupied e_g orbital of the Ir_3O_{12} trimer should be split into two singlets by the monoclinic distortion, which causes the $S = 0$ ground state of the filled HOMO level ($S_{trimer} = 0$). Therefore, the $Ir^{4.33+}{}_3O_{12}$ trimer does not contribute to the magnetic properties of $Ba_4LnIr_3O_{12}$ ($Ln =$ La, Nd–Gd, Dy–Lu), and both $Ba_4LaIr_3O_{12}$ and $Ba_4LuIr_3O_{12}$ are diamagnetic.[36]

In a similar way as the case for the Ir_3O_{12} trimer, the electron configuration of the $Ru^{4.33+}{}_3O_{12}$ trimer (the number of 4d electrons is 11) with D_{3h} point symmetry is $(a_{1g})^2(e_g)^4(a_{2u})^2(e_u)^3$ and the schematic energy level diagrams are illustrated in Fig. 12(a).

Table 3. Summary of magnetic properties of 12L-$Ba_4LnM_3O_{12}$

Ln	Oxidation state of Ln	Magnetic properties (Transition temperature/K)	
		$Ba_4LnRu_3O_{12}$	$Ba_4LnIr_3O_{12}$
La	3+	AF (6.0)	Dia
Ce	4+	CW	AF (10.5)
Pr	4+	AF (2.4)	AF (35)
Nd	3+	F (11.0)	CW
Sm	3+	AF (3.2)	van Vleck
Eu	3+	AF (4.0)	van Vleck
Gd	3+	AF (2.5)	CW
Tb	4+	AF (24)	AF (16)
Dy	3+	AF (30)	CW
Ho	3+	AF (8.5)	CW
Er	3+	AF (8.0)	CW
Tm	3+	AF (8.0)	CW
Yb	3+	AF (4.8)	CW
Lu	3+	AF (8.0)	Dia

Note: AF; antiferromagnetic, F; ferromagnetic, Dia; diamagnetic; CW; Curie–Weiss.

Table 4. Effective magnetic moments of $Ba_4LnM_3O_{12}$ (Ln = La–Lu; M = Ru, Ir)

Ln	Electron configuration	$Ba_4LnRu_3O_{12}$		$Ba_4LnIr_3O_{12}$	
		μ_{eff} (μ_B)	μ_{cal} (μ_B)	μ_{eff} (μ_B)	μ_{cal} (μ_B)
La^{3+}	$4f^0$	2.86	1.73[*1]	Dia	Dia
Ce^{4+}	$4f^0$	5.01	—	1.61	1.73[*5]
Pr^{4+}	$4f^1$	5.85	5.52[*2]	2.94	3.07[*5]
Nd^{3+}	$4f^3$	4.70	4.01[*1]	3.60	3.62[*6]
Sm^{3+}	$4f^5$	2.88	2.29[*3]	—	—
Eu^{3+}	$4f^6$	1.18	1.73[*3]	—	—
Gd^{3+}	$4f^7$	8.24	8.13[*1]	7.98	7.94[*6]
Tb^{4+}	$4f^7$	8.78	9.33[*4]	8.02	8.13[*5]
Dy^{3+}	$4f^9$	11.20	10.77[*1]	10.71	10.63[*6]
Ho^{3+}	$4f^{10}$	10.79	10.74[*1]	10.36	10.60[*6]
Er^{3+}	$4f^{11}$	9.72	9.74[*1]	9.21	9.59[*6]
Tm^{3+}	$4f^{12}$	7.75	7.77[*1]	7.31	7.57[*6]
Yb^{3+}	$4f^{13}$	4.70	4.86[*1]	3.86	4.54[*6]
Lu^{3+}	$4f^{14}$	2.86	1.73[*1]	Dia	Dia

Note: [*1]: calculated moments for Ln^{3+} and $S = 1/2$,
[*2]: $\mu_{cal} = \sqrt{3 \times \mu^2_{Ru^{4+}} + \mu^2_{Pr^{4+}}}$,
[*3]: these values are calculated using the susceptibilities of Ln^{3+} ions at room temperature,
[*4]: $\mu_{cal} = \sqrt{3 \times \mu^2_{Ru^{4+}} + \mu^2_{Tb^{4+}}}$,
[*5]: calculated moments for Ln^{4+} and $S = 1/2$,
[*6]: free ion values for Ln^{3+}.

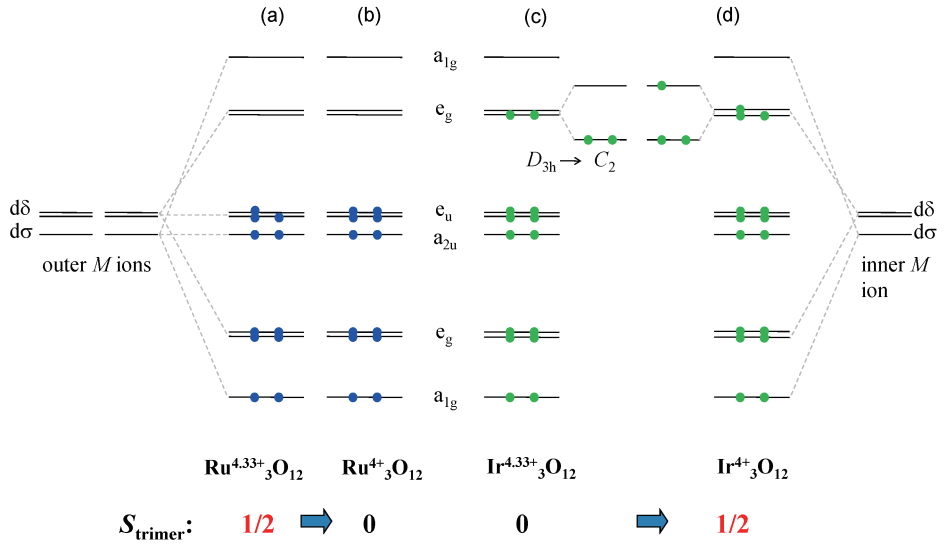

Fig. 12. Qualitative molecular orbital diagram for M_3O_{12} trimer in the $Ba_4LnM_3O_{12}$ (M = Ru, Ir).

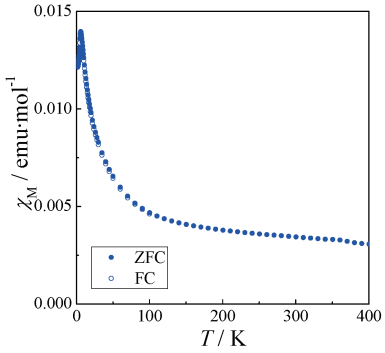

Fig. 13. Temperature dependence of the magnetic susceptibility for $Ba_4LaRu_3O_{12}$.

The highest occupied e_u orbital has the $S = 1/2$ ground state. Therefore, the $Ru^{4.33+}{}_3O_{12}$ trimer ($S_{trimer} = 1/2$) contributes to the magnetic properties of $Ba_4LnRu_3O_{12}$. **Figure 13** shows the temperature dependence of the magnetic susceptibility for $Ba_4LaRu_3O_{12}$. Both $Ba_4LaRu_3O_{12}$ and $Ba_4LuRu_3O_{12}$ order antiferromagnetically at 6.0, and 8.0 K, respectively. Since La^{3+} and Lu^{3+} ions are diamagnetic, the $Ru^{4.33+}{}_3O_{12}$ trimers are antiferromagnetically coupled. Other $Ba_4LnRu_3O_{12}$ compounds show similar antiferromagnetic transitions at comparable temperatures, which should be due to the magnetic ordering of the $Ru^{4.33+}{}_3O_{12}$ trimers.

5.2 Magnetic properties of $Ba_4Ln^{4+}M^{4+}{}_3O_{12}$

Table 3 shows that the magnetic behavior is contrastive between two compounds $Ba_4CeM_3O_{12}$ (M = Ru, Ir), i.e., the iridium-containing compound $Ba_4CeIr_3O_{12}$ antiferromagnetically orders at 10.5 K, while the ruthenium-containing compound $Ba_4CeRu_3O_{12}$ shows no magnetic ordering down to 0.5 K. Since the tetravalent Ce^{4+} ion is diamagnetic, only the M^{4+} ions (i.e., Ru^{4+} and Ir^{4+} ions) contribute to the magnetic properties of $Ba_4CeM_3O_{12}$ compounds, and this magnetic behavior of $Ba_4Ln^{4+}M^{4+}{}_3O_{12}$ is understandable by considering the magnetic properties of $M^{4+}{}_3O_{12}$ trimer.

In the same way as the case of $Ir^{4.33+}{}_3O_{12}$, the $Ir^{4+}{}_3O_{12}$ trimer has fifteen 5*d* electrons, and its electron configuration is $(a_{1g})^2(e_g)^4(a_{2u})^2(e_u)^4(e_g)^3$ [see Fig. 12(d)]. The highest occupied e_g orbitals (doublet) have the $S = 1/2$ ground state. The antiferromagnetic ordering of $Ba_4CeIr_3O_{12}$ is due to this ground $S = 1/2$ state. On the other hand, the electron configuration of the $Ru^{4+}{}_3O_{12}$ trimer is $(a_{1g})^2(e_g)^4(a_{2u})^2(e_u)^4$, indicating the $S = 0$ ground state of the filled HOMO, as shown in Fig. 12(b). Therefore, $Ba_4CeRu_3O_{12}$ should be diamagnetic and shows no magnetic ordering. Actually it is weakly paramagnetic, indicating that the molecular orbital model is not perfect for the case of Ru_3O_{12} trimer. We have to consider the excited state. This is because the 4*d* electrons are somewhat more localized than the 5*d* electrons.[42)]

As listed in Table 3, magnetic susceptibility measurements for $Ba_4PrRu_3O_{12}$ and $Ba_4PrIr_3O_{12}$ show that an antiferromagnetic transition occurs at 2.4 and 35 K, respectively. Since $Ba_4CeRu_3O_{12}$ shows no long-range magnetic ordering down to 0.5 K, the magnetic anomaly observed at 2.4 K in $Ba_4PrRu_3O_{12}$ is due to the magnetic interactions of the magnetic moment of Pr^{4+} ions. The results of the specific heat measurements and evaluation of the magnetic entropy change due to the antiferromagnetic ordering have quantitatively cleared this point.[35)]

Figure 14 illustrates that the magnetic structure of $Ba_4TbRu_3O_{12}$ at 2.5 K. The magnetic moments of Tb and Ru ions are collinear and lie on the *ab* plane. The Ru moments in the Ru_3O_{12} trimer order ferrimagnetically. Along the *c*-axis, each of the magnetic moments for Tb and Ru ions are alternately stacked.[35)]

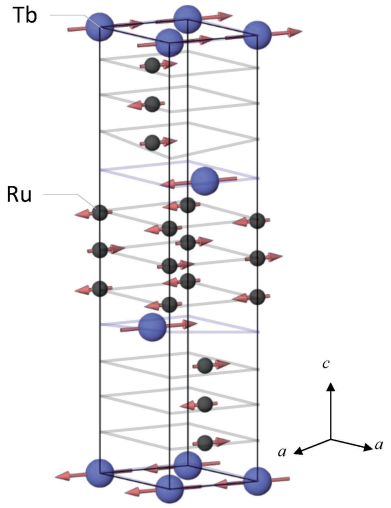

Fig. 14. Magnetic structure of $Ba_4TbRu_3O_{12}$ at 2.5 K.

6. Summary

Structures and magnetic properties of the general formula $A_nLnM_{n-1}O_{3n}$ (A = alkaline earth elements; Ln = rare earths; M = Ru, Ir; n = 1–4) have been studied. For the double perovskites $ALnMO_6$, antiferromagnetic transitions due to the magnetic cooperative phenomena between d and f electrons have been observed at relatively high temperatures. For n = 3, 6L-perovskite type compounds $Ba_3LnM_2O_9$ are formed. Peculiar temperature-dependence of the magnetic susceptibility has been found, which is explained by the d–f magnetic interactions and the magnetic coupling between M ions in the M_2O_9 dimer. For n = 4, quadruple perovskites $Ba_4LnM_3O_{12}$ with 12 layers are formed, in which M_3O_{12} trimer and LnO_6 octahedra are alternately linked by corner-sharing. Their magnetic behavior has been well explained by the number of d electrons in the M_3O_{12} trimer and magnetic properties of Ln ions.

References

1) K. Ito, K. Tezuka and Y. Hinatsu, *J. Solid State Chem.*, **157**, 173–179 (2001).
2) A. J. Jacobson, B. C. Tofield and B. E. F. Fender, *Acta Crystallogr., Sect. B: Struct. Crystallogr. Cryst. Chem.*, **28**, 956–961 (1972).
3) B. C. Tofield, A. J. Jacobson and B. E. F. Fender, *J. Phys., C*, **5**, 2887–2895 (1972).
4) Y. Hinatsu, M. Ito and N. Edelstein, *J. Solid State Chem.*, **132**, 337–341 (1997).
5) K. Tezuka, Y. Hinatsu, Y. Shimojo and Y. Morii, *J. Phys.: Condens. Matter*, **10**, 11703–11712 (1998).
6) Y. Hinatsu and N. Edelstein, *J. Solid State Chem.*, **112**, 53–57 (1994).
7) Y. Hinatsu, *J. Solid State Chem.*, **100**, 136–140 (1992).
8) M. Bickel, G. L. Goodman, L. Soderholm and B. Kanellakopulos, *J. Solid State Chem.*, **76**, 178–185 (1988).
9) P. D. Battle, J. B. Goodenough and R. Price, *J. Solid State Chem.*, **46**, 234–244 (1983).
10) P. D. Battle and W. J. Macklin, *J. Solid State Chem.*, **52**, 138–145 (1984).
11) P. D. Battle and C. W. Jones, *J. Solid State Chem.*, **78**, 108–116 (1989).

12) P. D. Battle, C. W. Jones and F. Studer, *J. Solid State Chem.*, **90**, 302–312 (1991).
13) Y. Doi and Y. Hinatsu, *J. Phys.: Condens. Matter*, **11**, 4813–4820 (1999).
14) M. Wakeshima, D. Harada and Y. Hinatsu, *J. Alloys Compd.*, **287**, 130–136 (1999).
15) D. Harada, M. Wakeshima and Y. Hinatsu, *J. Solid State Chem.*, **145**, 356–360 (1999).
16) M. Wakeshima, D. Harada and Y. Hinatsu, *J. Solid State Chem.*, **147**, 618–623 (1999).
17) Y. Doi, Y. Hinatsu, K. Oikawa, Y. Shimojo and Y. Morii, *J. Mater. Chem.*, **10**, 797–800 (2000).
18) Y. Izumiyama, Y. Doi, M. Wakeshima, Y. Hinatsu, K. Oikawa, Y. Shimojo and Y. Morii, *J. Mater. Chem.*, **10**, 2364–2367 (2000).
19) M. Wakeshima, D. Harada and Y. Hinatsu, *J. Mater. Chem.*, **10**, 419–422 (2000).
20) Y. Izumiyama, Y. Doi, M. Wakeshima, Y. Hinatsu, Y. Shimojo and Y. Morii, *J. Phys.: Condens. Matter*, **13**, 1303–1313 (2001).
21) Y. Sasaki, Y. Doi and Y. Hinatsu, *J. Mater. Chem.*, **12**, 2361–2366 (2002).
22) Y. Izumiyama, Y. Doi, M. Wakeshima, Y. Hinatsu, A. Nakamura and Y. Ishii, *J. Solid State Chem.*, **169**, 125–130 (2002).
23) Y. Doi, Y. Hinatsu, A. Nakamura, Y. Ishii and Y. Morii, *J. Mater. Chem.*, **13**, 1758–1763 (2003).
24) K. Yamamura, M. Wakeshima and Y. Hinatsu, *J. Solid State Chem.*, **179**, 605–612 (2006).
25) R. Saez-Puche, E. Climent-Pascual, R. Ruiz-Bustos, M. A. Alario-Franco and M. T. Fernandez-Diaz, *Prog. Solid State Chem.*, **35**, 211–219 (2007).
26) M. Wakeshima, Y. Hinatsu and K. Ohoyama, *J. Solid State Chem.*, **197**, 236–241 (2013).
27) C. Sakai, Y. Doi and Y. Hinatsu, *J. Alloys Compd.*, **408**, 608–612 (2006).
28) J. M. Longo and J. A. Kafalas, *J. Solid State Chem.*, **1**, 103–108 (1969).
29) Y. Doi, K. Matsuhira and Y. Hinatsu, *J. Solid State Chem.*, **165**, 317–323 (2002).
30) Y. Doi, M. Wakeshima, Y. Hinatsu, A. Tobo, K. Ohoyama and Y. Yamaguchi, *J. Mater. Chem.*, **11**, 3135–3140 (2001).
31) Y. Doi, Y. Hinatsu, Y. Shimojo and Y. Ishii, *J. Solid State Chem.*, **161**, 113–120 (2001).
32) C. H. De Vreugd, H. W. Zandbergen and D. J. W. IJdo, *Acta Crystallogr., Sect. C: Cryst. Struct. Commun.*, **40**, 1987–1989 (1984).
33) A. F. Fuentes, K. Boulahya and U. Amador, *J. Solid State Chem.*, **177**, 714–720 (2004).
34) N. Creon, C. Michel, M. Hervieu, A. Maignan and B. Raveau, *Solid State Sci.*, **5**, 243–248 (2003).
35) Y. Shimoda, Y. Doi, Y. Hinatsu, K. Ohoyama and Y. Yamaguchi, *Chem. Mater.*, **20**, 4512–4518 (2008).
36) Y. Shimoda, Y. Doi, M. Wakeshima and Y. Hinatsu, *J. Solid State Chem.*, **182**, 2873–2879 (2009).
37) A. F. Wells, "Structural Inorganic Chemistry", 5th Ed., Oxford Clarendon Press (1984).
38) R. D. Shannon, *Acta Crystallogr., Sect. A: Found. Crystallogr.*, **32**, 751–767 (1976).
39) Y. Shimoda, Y. Doi, M. Wakeshima and Y. Hinatsu, *Inorg. Chem.*, **48**, 2104–2110 (2009).
40) Y. Shimoda, Y. Doi, M. Wakeshima and Y. Hinatsu, *J. Solid State Chem.*, **183**, 33–40 (2010).
41) B. E. Bursten, F. A. Cotton and A. Fang, *Inorg. Chem.*, **22**, 2127–2133 (1983).
42) Y. Shimoda, Y. Doi, M. Wakeshima and Y. Hinatsu, *J. Solid State Chem.*, **183**, 1962–1969 (2010).

Yukio Hinatsu graduated from Osaka University in 1977 with a B.E. degree in nuclear engineering. He received his Ph. D. degree in nuclear engineering from Osaka University in 1982. After graduation, he joined the Japan Atomic Energy Research Institute as a Research Scientist. He studied the chemical behavior of fission products from the nuclear spent fuel at the Oak Ridge National Laboratory in Tennessee, USA, as a visiting scientist for one and half years in 1988–1989. Then, he moved to California and studied the electronic state of actinide ions in solids, at the Lawrence Berkeley Laboratory, University of California at Berkeley for a year in 1989–1990. Since 1995, he has been a full Professor of the Division of Chemistry, Faculty of Science, Hokkaido University.